STM JOURNALS

Journal of
Polymer & Composites

ISSN: 2321-2810 (Online)
ISSN: 2321-8525 (Print)
Volume 12, Special Issue 2, 2024
DOI (Journal): 10.37591/JoPC

http://engineeringjournals.stmjournals.in/index.php/JoPC/index

Research JoPC

Rotational Speed Influence on Weld Temperature in Friction Stir Lap Joint of Aluminium Alloy 6061 Using Numerical Simulation

Amit Yadav[1,*], Ajai Jain[2], Rajiv Verma[3]

Abstract

The weld quality assessment in friction stir welding depends on the choice of suitable weld parameters. Rotational speed is one such parameter. The study utilizes a computational fluid dynamics model to examine the influence of various rotational on the workpiece and weld interface temperature. The workpiece selected for this study is an Aluminium Alloy 6061, while the tool employed is a truncated conical pin tool featuring a conical shoulder in a lap joint configuration. The maximum weld interface temperature rises linearly with a relatively constant slope from 500RPM to 2900RPM rotational speed, according to the study. With increase in rotational speed, most of the heat created is moved away to the trailing side of the workpiece due to material flow; therefore, heat transferred down the thickness is minimal. The validation of the findings of this investigation is accomplished through a comparative analysis with data that has been previously published. Given the aforementioned facts and conclusions, friction stir welders can enhance their understanding of the influence of rotational-speed on the quality of welding.

Keywords: Friction stir weld, computational fluid-dynamics, ansys-fluent, finite-volume approach, numerical simulation

INTRODUCTION

The Friction Stir Welding (FSW) technique was initially developed in 1991 and subsequently patented by the prestigious organization known as The Welding Institute (TWI) [1]. The purpose of this invention was to achieve robust and durable structures by welding materials with limited welding capabilities, specifically Aluminium alloys. This issue is of great importance to various industries, particularly the aerospace sector, as conventional methods are inadequate for welding Aluminium alloys or joining incompatible materials like Aluminium and Magnesium alloys.

***Author for Correspondence**
Amit Yadav

[1]Research Scholar, Department of Mechanical Engineering, National Institute of Technology Kurukshetra, India
[2]Professor, Department of Mechanical Engineering, National Institute of Technology Kurukshetra, India
[3]Associate Professor, Department of Mechanical Engineering, National Institute of Technology Kurukshetra, India

Received Date: March 21, 2024
Accepted Date: April 18, 2024
Published Date: May 16, 2024

Citation: Amit Yadav, Ajai Jain, Rajiv Verma. Rotational Speed Influence on Weld Temperature in Friction Stir Lap Joint of Aluminium Alloy 6061 Using Numerical Simulation. Journal of Polymer & Composites. 2024; 12(Special Issue 2): S235–S245p.

During FSW, a rotating tool is gradually inserted into the workpiece until the shoulder comes into contact with the workpiece, as shown in Figure. 1. This position is upheld until the necessary temperature is attained due to the generation of heat through friction and plastic deformation. In order to accomplish the necessary weld, the tool is displaced along the weld line. The term advancing side (AS) is used to describe the side of a rotating tool that has identical direction as the tangential velocity and traverse speed (TRS). The retreating side (RS) refers to the side of a rotating tool that has a vectorial sense opposite to the tangential velocity and TRS [2]. The workpiece section located ahead of tool is known as leading side, and the section located behind tool is known as trailing side.

Since its inception, a substantial body of research has been dedicated to investigating the impacts of various elements in the FSW process. Certain factors are machine-specific, while others, such as spinning velocity and pin geometry, are inherent to the tool [3–8]. Each of these variables influences the transfer of heat and the movement of material, which subsequently has an effect on the microstructure and quality of the weld [9,10]. This study aims to assess the influence of rotational-speed (ROS) on weld temperature for Aluminium alloy 6061 (AA6061) lap welds using a truncated conical pin with conical shoulder (TCPCS) tool. This study employs the finite volume technique (FVM) of computational fluid dynamics (CFD) as an efficient and time-effective approach (11).

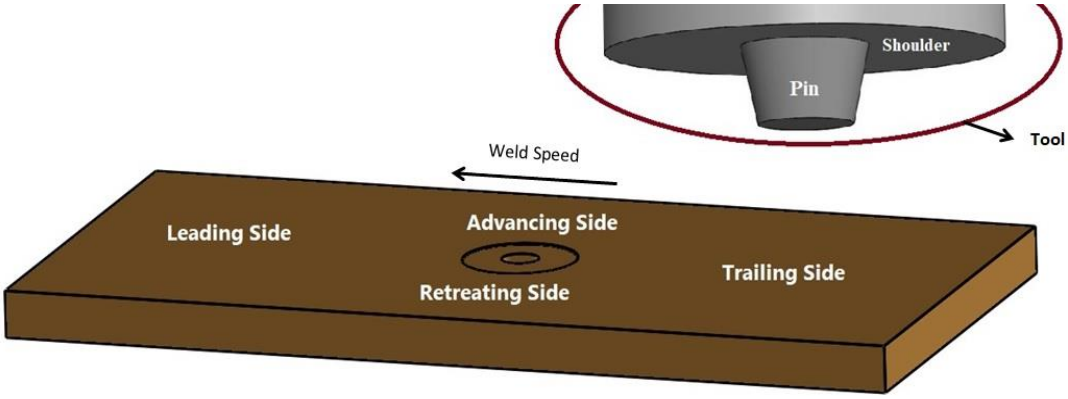

Figure 1. Friction stir weld process

LITERATURE REVIEW

Multiple researchers have conducted investigations on FSW. Nandan et al. 2006; Nandan et al. 2006; Nandan et al. 2007 utilised the three-dimensional visco plastic model for butt joints in stainless steel-SS304, AA6061, and mild steel-1018, respectively. The instrument's combined rotational and linear movement revealed a notable imbalance in the temperature distribution surrounding it [12–14]. Z. Zhang and Zhang 2008 conducted a study where they developed a three-dimensional thermo-mechanical model to examine the temperature and material flow in the butt weld of AA6061-T6. Augmenting the ROS while reducing the welding speed results in an intensified stirring motion, hence improving the weld's quality. To avoid defects, the ROS should increase proportionally with the welding speed [15]. J. Zhang et al., 2014 developed a CFD model in FLUENT® to analyse the temperature distribution and material flow characteristics of an AA6061-T6 lap joint under the influence of a conical tool. The model does not consider the effect of tool tilt. The findings suggest that the shoulder surface area is primarily responsible for the majority of heat generation, accounting for 88% of the total. On the other hand, the regions of the pin's side surface and bottom surface barely account for 10.48% and 1.52%, respectively. The occurrence of intense material movement is primarily limited to the area near the tool, where material located on tool's front is driven towards RS and then gathers at tool's back [11]. Jain, Pal, and Singh 2016 created a model to forecast the forces, spindle torque, temperature, and plastic strain that occur during the butt-welding process of two AA2024-T4 metals. The rise in heat generation rate, as indicated by the temperature distribution, leads to a decrease in forces and spindle torque as the ROS increases. In addition, the conical shape of the pin resulted in a higher material velocity compared to its cylindrical version while requiring less effort during the plunging process [16]. In their study, Shi & Wu, 2017 created a transient model to accurately assess the dynamic changes in heat, temperature and material-flow during the butt FSW of AA2024. They also examined how these factors are influenced by process parameters, including TRS and tool ROS. It has been observed that the tool torque rises when the TRS increases, providing that the ROS remains constant. An inverse relationship was seen when the rotating speed increased, assuming that the temperature and pressure remained constant [17]. Hasan, 2019 conducted a study where he used FSW to simulate the butt joint of AZ31 magnesium alloy. Results showed that the maximum temperature drops as the TRS increases, while the ROS remains constant [18]. Roubaiy et al., 2020 examined how different welding parameters affect the mechanical properties of a butt joint made by FSW, using aluminium 5083-H116. As the

ROS increases (assuming the TRS remains constant), the tensile strength and joint efficiency rise, while the absorbed energy drops. Conversely, a contrasting effect on TRS was noticed, but the ROS remained unchanged [19]. Nirmal & Jagadesh, 2020 conducted a study on the percentage elongation, yield strength, and ultimate tensile strength of a dual-phase titanium alloy using FSW on butt joints. The study revealed that when the ROS increases (assuming the TRS remains constant), the yield stress, ultimate tensile stress, and tensile strength also increase, while the percentage elongation drops. An inverse relationship was seen as the TRS increased, assuming the ROS remained constant [20]. Andrade et al., 2020 examined the torque and temperature FSW of aluminium alloys belonging to series AA2xxx, AA5xxx, AA7xxx, and AA8xxx. It has been observed that when the ROS increases (assuming the torque sensitivity remains constant), the torque drops but the peak temperature increases. In contrast, there was a reported increase in TRS, assuming that the rotating speed remained constant. Furthermore, it was noted that an increase in workpiece thickness correspondingly leads to an increase in torque. An augmentation in shoulder diameter leads to a corresponding augmentation in peak torque and temperature [21]. H. J. Zhang et al., 2020 performed FSW on AA6061 with rotation speeds varying from 1,000 to 6,000 RPM. The study reveals that as the ROS increases (while keeping the TRS constant), the peak temperature also increases [22]. Yadav et al., 2023 conducted a study on the tool tilt effect for AA6061 using a tapered cylindrical pin to analyse its impact on heat and material flow. It was discovered that the temperature drops as the tilt angle increases [23].

The literature review indicates that no previous study has examined the influence of different ROS on weld temperature for AA6061. Specifically, this study focuses on the use of a TCPCS tool for a lap joint. The current study investigates the impact of different ROSs (ranging from 500 to 2900 RPM). Solidworks® 2017 is utilised for the purpose of geometric modeling, whereas the CFD program FLUENT® is employed specifically for FVM numerical modeling [24]. The novelty of this work will be elucidated in the next section.

This study examines the impact of tilt angle and slip in lap weld. The impact of the shoulder's side surface on heat generation is also taken into account. The transient strategy is being evaluated. An analysis is conducted on the performance metrics of the lap weld's weld surface. Prior studies have examined the maximum temperature attained within a workpiece. The range of ROS is dictated by the recrystallization and solidus temperatures of the workpiece formed at the weld surface.

Numerical Modeling

As a result of the intricate nature of the practical arrangement, a cost and time-efficient technique of numerical modeling is utilised [12,25]. This portion provides a numerical model for friction stir lap weld of AA6061 using a TCPCS tool. It includes the necessary assumptions, boundary-conditions, material-parameters and model validation.

Description of Model

Utilising numerical modeling allows for the efficient and effortless visualisation of temperature distribution, material movement, as well as stress and strain analysis [11]. It offers a valuable understanding of the operation of the process. Figure. 2 illustrates the simulation model. AA6061 plates are utilised. The dimensions of each plate are 200mm x 100mm x 5mm. When joined in a lap arrangement, the measurements are 200mm x 100mm x 10mm [11]. The parameters for the FSW technique are provided in Table 1. The selection of these characteristics is based on a thorough evaluation of the pertinent literature [10,11].

The Realisable k-epsilon viscous model is employed to simulate the flow of material in a transient state. Mesh with tetrahedron-cells is utilised, with fine mesh at the interface between the tool and the workpiece, as depicted in Figure. 3. The present work adheres to the following assumptions: The process is a quasi-steady process, meaning that the rate of heat generation remains constant. Plasticized material is classified as non-Newtonian, incompressible, and visco-plastic. The material is presumed to

exhibit the characteristics of a non-Newtonian fluid, where its viscosity is influenced by both temperature and strain rate. There is a condition of partial slip between the tool and the workpiece. The upper, bottom, and side surfaces of the workpiece have a free slip condition. The outlet boundary assumes a value of zero pressure.

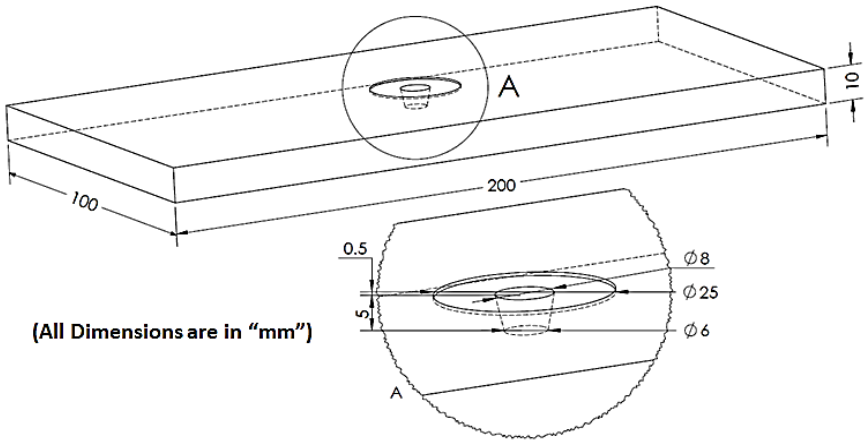

Figure 2. Model's schematic sketch

Table 1. FSW Process Parameters in the Present Work

Process Parameter	Value
Diameter of Shoulder	25mm
Conical angle of shoulder	2°
Tilt Angle	1.5°
Pin length	5mm
Conical-pin root diameter	8mm
Conical-pin tip diameter	6mm
Traverse Speed	0.05m/s
Plunge depth	1.5mm

Boundary Conditions and Material Properties

In order to make precise predictions about weld performance, it is crucial to employ realistic boundary conditions [18]. Figure. 4 displays the parts and boundaries imposed on the model.

The inlet boundary condition of flow is defined as follows:

$$u = u_{weld}, v = 0, w = 0 \quad (1)$$

where weld velocity is represented by u_{weld}, whereas the velocity intensities in the X, Y, and Z directions are represented by u, v, and w, respectively.

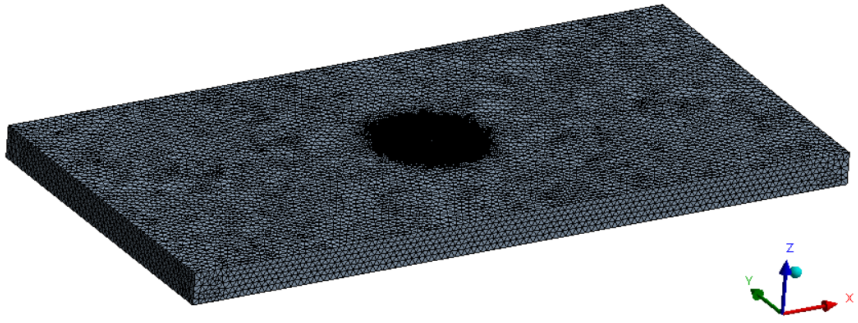

Figure 3. Mesh used

The tool periphery velocity, which is the combined effect of the tool's angular velocity and the welding speed, is provided below:

$$u_i = \omega r\sin\theta - u_{weld},\ v_i = \omega r\cos\theta,\ w_i = 0 \quad (2)$$

The value of r is such that $r_1 < r < r_3$. The variables u_i denote velocity vector in x-direction, v_i denote velocity vector in y-direction, and w_i denote velocity vector in z-directions. r_1 represents the radius of tool shoulder; r_3 represents the radius of pin bottom; θ is the angle between the horizontal direction vector from the tool axis to any point on the cylindrical surface. In the weld direction, θ is equal to zero.

Tool periphery velocity when tool tilt angle (ξ) and contact state variable (δ) are considered are represented by Equation.

$$u_i = (1-\delta)((\omega r sin\theta)\cos\xi - u_{weld}) \quad (3)$$
$$v_i = (1-\delta)\omega r cos\theta \quad (4)$$
$$w_i = (1-\delta)(\omega r sin\theta)\sin\xi \quad (5)$$
$$\delta = 0.9\left(0.31e^{\omega r/1.87} - 0.026\right) \quad (6)$$
$$\eta\ (viscosity) = \frac{\sigma}{3\bar{\varepsilon}} \quad (7)$$
$$\sigma\ (\text{flow stress}) = \frac{1}{\beta}\ln\left\{\left(\frac{Z}{A}\right)^{\frac{1}{n}} + \left(1+\left(\frac{Z}{A}\right)^{\frac{2}{n}}\right)^{\frac{1}{2}}\right\} \quad (8)$$
$$Z\ (\text{Zener Hollomon parameter}) = \bar{\varepsilon}e^{\left(\frac{Q}{RT}\right)} \quad (9)$$
$$\bar{\varepsilon}\ (\text{strain rate}) = \left(\frac{2}{3}\varepsilon_{ij}\varepsilon_{ij}\right)^{\frac{1}{2}} \quad (10)$$

where T represents temperature, measured in Kelvin (K). A, β, and n are constants that describe the material properties. Q is an activation energy that does not depend on temperature. R is the gas constant [26, 27 and 28]. These equations are implemented through the use of User Defined Functions (UDF). The Table 2 provides the material-constants and properties of AA6061 [29].

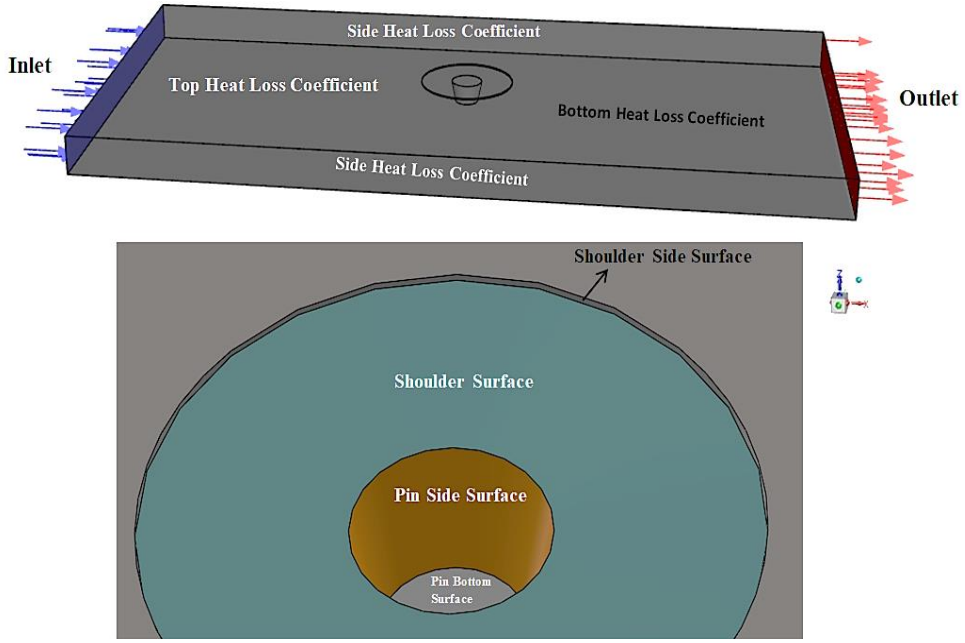

Figure 4. Model's parts and boundary conditions

Table 2. Material-Constants and Properties for Aluminum Alloy 6061

Parameter	Value
Material- constants:A (s^{-1})nQ ($J.mol^{-1}$)B (MPa)	2.41×10^{8} 3.551.45$\times10^{5}$ 0.045
Material density, ρ ($kg.m^{-3}$)	2700
Gas constant, R ($J.K^{-1}.mol^{-1}$)	8.314

The heat created during the FSW process is distributed over many regions. The tool's contacting surface with the workpiece has been partitioned into three sections: shoulder surface (SS), side surface of pin (P_{SS}), and bottom surface of pin (P_{BS}), as seen in Figure. 4. The SS is subdivided into two sections: shoulder with conical surface (S_{CS}) and shoulder with flat surface (S_{FS}). All these sections exhibit partial sticking-sliding contact. The heat produced by different sources is provided below:

$$Q_{total} = \delta Q_{sticking} - (1-\delta)Q_{sliding} \tag{11}$$

The symbol δ represents the contact state variable. When the slip coefficient (δ) is equal to zero, heat is only generated through friction. When the value of δ is equal to 1 (indicating a stick), all heat is produced only through the deformation of the plastic material [30].

The assumed maximum yielding shear stress is:

$$\tau_b = \frac{\sigma_s}{\sqrt{3}} \tag{12}$$

where σ_s represents the material's yield stress at its melting point temperature [31]**.**

The δ at S_{CS} has been assigned a value of 0.35 [11]. The heat-flux (W/m^2) at this section is:

$$q_{S_{CS}} = \frac{[\delta_{CSS}\tau_b+(1-\delta_{CSS})\mu P]2\omega[(r_1^3-r_2^3)(1+\tan\propto')]}{3(r_1^2-r_2^2)} \tag{13}$$

At P_{SS}, δ is equal to 0.5 [11]. The heat-flux (W/m^2) at this section is:

$$q_{P_{SS}} = \frac{2\delta_{PSS}\omega\tau_b(r_2^3-r_3^3)cos\alpha}{3(r_2^2-r_3^2)} + \frac{2(1-\delta_{PSS})\mu P\omega(r_2^3-r_3^3)}{3(r_2^2-r_3^2)} \tag{14}$$

At P_{BS}, δ has a value of 0.35 [11]. The heat-flux (W/m^2) at this section is:

$$q_{P_{BS}} = \frac{2\omega r_3(\delta_{PBS}\tau_b+(1-\delta_{PBS})\mu P)}{3} \tag{15}$$

where μ is coefficient of friction [11]; P is plunge pressure (Pa); ω is ROS (rad/s) and $\propto'$ is cone angle of shoulder ($\propto' = 0$ for S_{FS})). A plunging pressure of 12MPa is taken here [11].

The specific-heat C_p equation for AA6061 is shown below [13].

$$C_p = 929 - 0.627T + 1.481\times10^{-3}T^2 - 4.33\times10^{-8}T^3 \tag{16}$$

The thermal conductivity k equation for AA6061 is shown below.

$$k = 25.22 + 0.3978T + 7.358\times10^{-6}T^2 - 2.518\times10^{-7}T^3 \tag{17}$$

The boundary condition for heat exchange between top surface of the workpiece and the environment is convective as well as radiative heat transfer [13]. The heat exchange between the bottom and side surfaces of the workpiece is conductive (due to contacts of jigs and fixtures) and convective heat transfer, respectively. All these heat exchanges are converted to convective form as shown below [13]:

$$k\frac{\partial T}{\partial z} = h_t(T-T_0) \tag{18}$$

$$k\frac{\partial T}{\partial z} = h_b(T-T_0) \tag{19}$$

$$k\frac{\partial T}{\partial z} = h_s(T - T_0) \quad (20)$$

where h_t, h_b and h_s are coefficients of heat dissipation at workpiece's top, bottom and side surface, respectively. T_0 is the environmental temperature (300K).

In this study, h_b = 150W/m^{2}K, and h_t = h_s = 80W/m^{2}K. The external emissivity of workpiece top surface is 0.09 [32].

Model Validation

Validation of current model is done with the work by J. Zhang et al., 2014. A three-dimensional CFD model was constructed to study the temperature and material-flow behaviour of an AA6061-T6 lap joint with a conical tool (ignoring tool tilt effect). In the present study, the above work is replicated, and upon validation of the current methodology and procedure, additional fixed input parameters (tilt angle and plunge depth) are introduced. The temperature distribution and material flow velocity data closely correspond to those reported data. Figure. 5 compares the present and validated studies' temperature distributions. Thus, numerical-modeling methods are satisfactory.

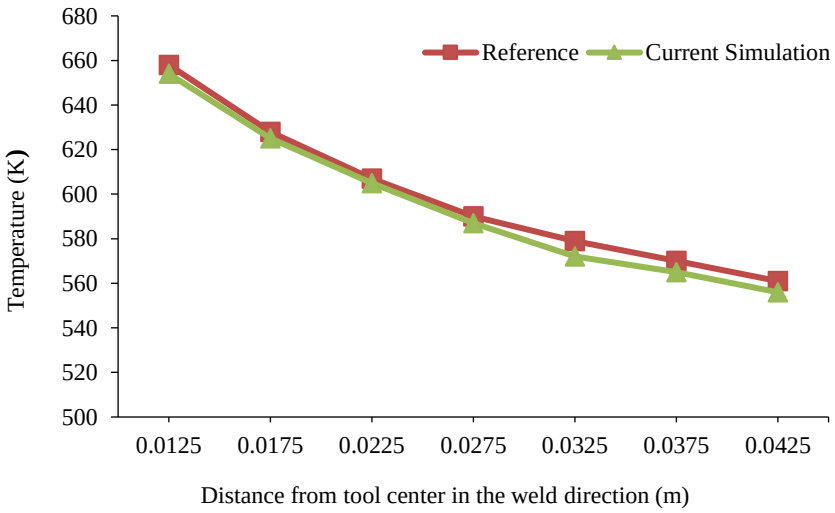

(a) Temperature at workpiece's top surface on trailing side

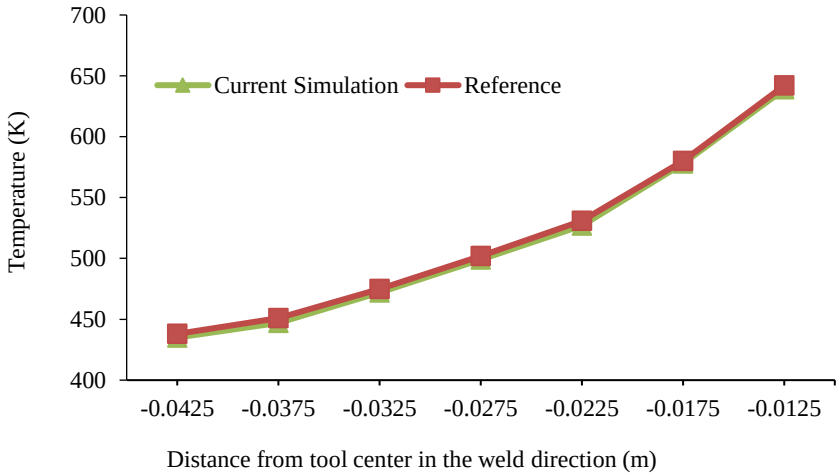

(b) Temperature at Workpiece's Top Surface on Leading Side

Figure 4. Comparison of Weld Temperature for Present and Reference Study (11)

RESULTS

This part of the article presents ROS's influence on maximum weld interface temperature as performance measures. The range of ROS is selected from 500RPM to 2900RPM range as below 500RPM ROS, temperature at weld surface (surface joining two weld plates in lap joint) reaches below its recrystallization temperature ((0.5*Melting point temperature) for alloys, i.e., 462.5K) and above 2900RPM ROS, temperature of workpiece increases above its solidus temperature (855K for AA6061).

Effect of Rotational Speed

To study effect of ROS on maximum weld interface temperature, all other input parameters such as TRS, tilt angle and plunge depth are kept at their average value of 0.05m/s, 0.25° and 0.375mm, respectively. Table 3 summarizes considered performance measures as varying ROS, which varies from 500RPM to 2900RPM.

Table 3. Effect of rotational speed on maximum weld interface temperature

Rotational Speed (RPM)	Max. Workpiece Temperature (K)	Max. Weld Interface Temperature (K)
500	454	379
900	544	427
1300	623	473
1700	692	516
2100	766	555
2500	826	591
2900	917	632

Figure. 6 below shows effect of ROS on maximum weld interface temperature. It is noticed that with an increase in ROS from 500RPM to 2900RPM, peak temperature increases linearly (with an almost constant slope). This is due to the fact that heat flux is directly proportional to ROS, keeping transfer speed, tilt angle and plunge depth constant (Equations 13, 14, and 15). As heat flux is dependent on ROS, with an increase in ROS, heat flux increases, and hence, the maximum weld interface temperature also increases**.**

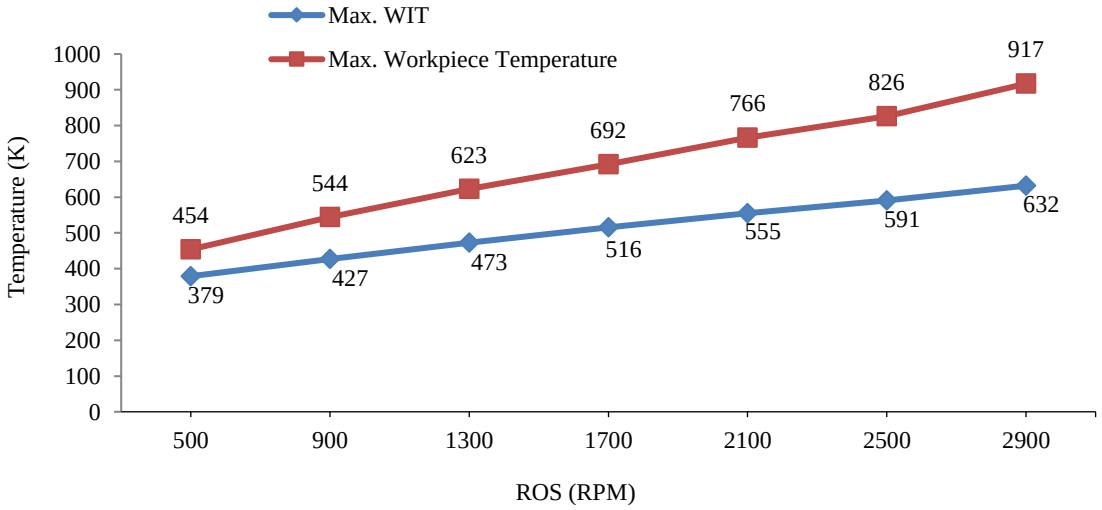

Figure 5. Rotational speed effect on maximum weld interface temperature

Percentage temperature change in workpiece and at weld interface (w.r.t. maximum workpiece temperature), increases with increase in rotational speed (Table 4). This is because; most of the heat generated is carried away to the trailing side of the workpiece due to flow of material in that direction [33]. Therefore, heat transferred down the workpiece thickness is less.

Table 4. Percentage Temperature Change in Workpiece and at Weld Interface w.r.t. Maximum Workpiece Temperature

Rotational Speed (RPM)	Max. Workpiece Temperature (K)	Max. Weld Interface Temperature (K)	Percentage Change in Temperature w.r.t. Maximum Workpiece Temperature (%)
500	454	379	16.51982
900	544	427	21.50735
1300	623	473	24.07705
1700	692	516	25.43353
2100	766	555	27.54569
2500	826	591	28.45036
2900	917	632	31.07961

The recommended ROS for achieving a sound weld on the specified workpiece shape is 2500 RPM, assuming all other input parameters remain constant. This is because the highest temperature that the workpiece may reach is lower than its solidus temperature i.e. 855K for AA6061. Furthermore, when the ROS is below 2500RPM, the temperature produced at the weld interface is reduced, leading to a decrease in the quality of the weld.

CONCLUSIONS

This investigation studies the effect of varying ROS on maximum weld interface temperature as performance measures. The following conclusions are drawn from the study:

- With an increase in ROS from 500RPM to 2900RPM, peak temperature increases with an almost constant slope, meaning an increasing linear trend.
- The maximum weld interface temperature is less than the maximum workpiece temperature generated.
- Percentage temperature change in workpiece and at weld interface (w.r.t. maximum workpiece temperature), increases with increase in rotational speed.
- The recommended ROS for achieving a sound weld on the specified workpiece shape is 2500 RPM.

REFERENCES

1. Al. T et. Friction welding. Weld J (Miami, Fla). 1995;78(4):56.
2. Nandan R, DebRoy T, Bhadeshia HKDH. Recent advances in friction-stir welding - Process, weldment structure and properties. Prog Mater Sci. 2008;53(6):980–1023.
3. Zhang XX, Wu LH, Andrä H, Gan WM, Hofmann M, Wang D, et al. Journal of Materials Science & Technology Effects of welding speed on the multiscale residual stresses in friction stir welded metal matrix composites. 2019;35:824–32.
4. Buffa G, Campanile G, Fratini L, Prisco A. Friction stir welding of lap joints : Influence of process parameters on the metallurgical and mechanical properties. 2009;519:19–26.
5. Keivani R, Bagheri B, Sharifi F, Ketabchi M, Abbasi M. Effects of pin angle and preheating on temperature distribution during friction stir welding operation. Trans Nonferrous Met Soc China [Internet]. 2013;23(9):2708–13. Available from: http://dx.doi.org/10.1016/S1003-6326(13)62788-0
6. Shi L, Wu CS, Liu HJ. The effect of the welding parameters and tool size on the thermal process and tool torque in reverse dual-rotation friction stir welding. Int J Mach Tools Manuf. 2015;91:1–11.
7. Kadian AK, Puri G, Das S, Biswas P. Effect of tool geometry and process parameters on the material flow of friction stir welding. IIT Guwahati. 2014.
8. Zhang S, Shi Q, Liu Q, Xie R, Zhang G, Chen G. Effects of tool tilt angle on the in-process heat transfer and mass transfer during friction stir welding. Int J Heat Mass Transf. 2018 Oct 1;125:32–42.

9. Sun Z, Wu CS, Kumar S. Determination of heat generation by correlating the interfacial friction stress with temperature in friction stir welding. J Manuf Process. 2018 Jan 1;31:801–11.
10. Zhai M, Wu CS, Su H. Influence of tool tilt angle on heat transfer and material flow in friction stir welding. J Manuf Process [Internet]. 2020;59(July):98–112. Available from: https://doi.org/10.1016/j.jmapro.2020.09.038
11. Zhang J, Shen Y, Li B, Xu H, Yao X, Kuang B, et al. Numerical simulation and experimental investigation on friction stir welding of 6061-T6 aluminum alloy. Mater Des. 2014;60:94–101.
12. Nandan R, Roy GG, Lienert TJ, Debroy T. Numerical modelling of 3D plastic flow and heat transfer during friction stir welding of stainless steel. Sci Technol Weld Join. 2006;11(5):526–37.
13. Nandan R, Roy GG, Debroy T. Numerical simulation of three dimensional heat transfer and plastic flow during friction stir welding. Metall Mater Trans A Phys Metall Mater Sci. 2006;37(4):1247–59.
14. Nandan R, Roy GG, Lienert TJ, Debroy T. Three-dimensional heat and material flow during friction stir welding of mild steel. Acta Mater. 2007 Feb;55(3):883–95.
15. Zhang Z, Zhang HW. Numerical studies on controlling of process parameters in friction stir welding. 2008;9(2005):241–70.
16. Jain R, Pal SK, Singh SB. A study on the variation of forces and temperature in a friction stir welding process : A finite element approach. J Manuf Process [Internet]. 2016;23:278–86. Available from: http://dx.doi.org/10.1016/j.jmapro.2016.04.008
17. Shi L, Wu CS. Transient model of heat transfer and material flow at different stages of friction stir welding process. J Manuf Process. 2017 Jan 1;25:323–39.
18. Hasan AF. CFD modelling of friction stir welding (FSW) process of AZ31 magnesium alloy using volume of fluid method. J Mater Res Technol. 2019 Apr 1;8(2):1819–27.
19. Roubaiy AOA-, Nabat SM, Dl A. ScienceDirect An Investigation into Friction Stir Welding of Aluminium Alloy 5083-H116 Similar Joints. Mater Today Proc [Internet]. 2020;22:2140–52. Available from: https://doi.org/10.1016/j.matpr.2020.03.281
20. Nirmal K, Jagadesh T. Materials Today : Proceedings Numerical simulations of friction stir welding of dual phase titanium alloy for aerospace applications. Mater Today Proc [Internet]. 2020;(xxxx). Available from: https://doi.org/10.1016/j.matpr.2020.10.300
21. Andrade DG, Leitão C, Dialami N, Chiumenti M, Rodrigues DM. Modelling torque and temperature in friction stir welding of aluminium alloys. 2020;182(May).
22. Zhang HJ, Sun SL, Liu HJ, Zhu Z, Wang YL. Characteristic and mechanism of nugget performance evolution with rotation speed for high-rotation-speed friction stir welded 6061 aluminum alloy. J Manuf Process [Internet]. 2020;60(November):544–52. Available from: https://doi.org/10.1016/j.jmapro.2020.10.081
23. Yadav A, Jain A, Verma R. Effect of tilt angle for conical pin tool with a conical shoulder on heat transfer and material flow using numerical simulation in friction stir welding. Mater Phys Mech. 2023;51(3):126–45.
24. Kumar A, Bansal SN, Chandraker R. Computational modeling of blast furnace cooling stave based on heat transfer analysis. Mater Phys Mech. 2012;15(1):46–65.
25. Arora A, Nandan R, Reynolds AP, DebRoy T. Torque, power requirement and stir zone geometry in friction stir welding through modeling and experiments. Scr Mater. 2009 Jan;60(1):13–6.
26. Thomas WM, Johnson KI, Wiesner CS. Friction stir welding-recent developments in tool and process technologies. Adv Eng Mater. 2003;5(7):485–90.
27. Sheppard T, Wright DS. Determination of flovv stress: Part 1 constitutive equation for aluminium alloys at elevated temperatures. 1979;(June).
28. Sheppard T, Jackson A. Constitutive equations for use in prediction of flo\N stress during extrusion of alurniniul11alloys. 1997;13(March).
29. Tello KE, Gerlich AP, Mendez PF. Constants for hot deformation constitutive models for recent experimental data. Sci Technol Weld Join. 2010 Apr 1;15(3):260–6.
30. Hamilton C, Dymek S, Sommers A. A thermal model of friction stir welding in aluminum alloys. Int J Mach Tools Manuf. 2008;48(10):1120–30.

31. Neto DM, Neto P. Numerical modeling of friction stir welding process: A literature review. Int J Adv Manuf Technol. 2013;65(1–4):115–26.
32. Yang CL, Wu CS, Lv XQ. Numerical analysis of mass transfer and material mixing in friction stir welding of aluminum/magnesium alloys. J Manuf Process. 2018 Apr 1;32:380–94.
33. Yadav A, Jain A, Verma R. Numerical Simulation of Friction Stir Welding Process to Investigate the Effect of a Conical Pin Tool with a Flat and Conical Shoulder on Heat Transfer. NanoWorld J. 2023;9(Special Issue 1):S239–4

